

Observation of full contrast icosahedral Bose-Einstein statistics in laser desorbed, buffer gas cooled C₆₀

Ya-Chu Chan,^{1,2} Lee R. Liu,^{1,3,*} Andrew Scheck,^{1,3} David J. Nesbitt,^{1,2,3} Jun Ye,^{1,3,†} and Dina Rosenberg^{1,3}

¹*JILA, National Institute of Standards and Technology and University of Colorado, Boulder, Boulder, CO 80309*

²*Department of Chemistry, University of Colorado, Boulder, CO 80309*

³*Department of Physics, University of Colorado, Boulder, CO 80309*

(Dated: June 25, 2024)

The quantum mechanical nature of spherical top molecules is particularly evident at low angular momentum quantum number J . Using infrared spectroscopy on the 8.4 μm rovibrational band of buffer gas cooled $^{12}\text{C}_{60}$, we observe the hitherto unseen $R(J = 0 - 29)$ rotational progression, including the complete disappearance of certain transitions due to the molecule's perfect icosahedral symmetry and identical bosonic nuclei. The observation of extremely weak C_{60} absorption is facilitated by a laser desorption C_{60} vapor source, which transfers 1000-fold less heat to the cryogenic buffer gas cell than a traditional oven source. This technique paves the way to cooling C_{60} and other large gas phase molecules to much lower temperatures, providing continued advances for spectral resolution and sensitivity.

Due to their strong intramolecular interactions, perfect rotational symmetries, and long-lived rotational and vibrational degrees of freedom, large molecules are interesting platforms for probing strongly correlated many body phenomena [1, 2] and quantum information processing [3–5]. Quantum state resolved infrared spectroscopy is the key to unlock these capabilities. Molecules beyond ~ 10 atoms, however, typically exhibit intrinsic spectral congestion in the usual infrared bands due to the rapidly increasing vibrational density of states with increasing energy and atom number [6, 7]. C_{60} is a notable exception: due to its rigidity and symmetry, it is the largest molecule for which quantum state resolution in the infrared was achieved [8]. Based on this result, a series of high resolution spectroscopic measurements have provided the clearest understanding of structure and dynamics of individual C_{60} molecules to date. By fitting high resolution spectra to effective molecular Hamiltonians, the spectroscopic constants for the ground and excited ($T_{1u}(3)$) vibrational states were determined [8]. Then, detailed studies of the collisions between C_{60} and a variety of atomic and molecular species explored the intramolecular pathways of energy relaxation through rotational and vibrational degrees of freedom [9]. The observation of ergodicity breaking in the rotational fine structure of C_{60} [1] offers a new perspective on emergent phenomena in mesoscopic quantum systems made possible by free rotations, rotation-vibration coupling and perfect rotational symmetry.

These results were obtained using a 900 K oven source coupled to a cryogenic buffer gas cell [6, 10, 11]. However, the significant heat load of the oven source constrained the rotational temperature to lie ~ 150 K and above, preventing the concentration of significant population into states of low angular momentum quantum number J [8].

At low J , some rotational states are completely forbidden for the totally symmetric nuclear spin species. Because of the high symmetry and 60 identical spinless bosonic nuclei of $^{12}\text{C}_{60}$, these forbidden states are completely absent from its infrared spectrum, providing arguably the most striking example of symmetry and quantum mechanical effects on spherical top spectra [12].

In this work, we develop a laser desorption vapor source to produce a colder sample of gas phase C_{60} . This allows us to measure the R branch rotational progression of $^{12}\text{C}_{60}$ from $J = 0 - 29$ and beyond using cavity-enhanced high resolution spectroscopy on the 8.4 μm rovibrational band, demonstrating complete absence of rotational transitions, as predicted by nuclear spin statistics. We characterize the rotational temperature of laser desorbed C_{60} and find that it reaches below 100 K using both Ar and He buffer gas cooling. Rotational and Doppler thermometry indicate that rotational and translational degrees of freedom are essentially thermalized. We also observe large signal from cold C_{60} with He buffer gas, indicating that in spite of the enormous mismatch in masses, small He- C_{60} rotational quenching cross section [9], and highly non thermal optical excitation by 532 nm photons, He is able to efficiently cool the vibrational, rotational, and translational degrees of freedom of laser desorbed C_{60} . Our specific laser desorption technique possesses several unique features that enable high sensitivity molecular spectroscopy: 1) three orders of magnitude reduction in heat load on the cryogenic buffer gas cell compared to a traditional oven source; 2) stable pulse-to-pulse desorption yield, varying by less than 10%, due to the uniformity of the deposited C_{60} film thickness; 3) the use of unusually long duration (200 ms) and low peak power (2 W) desorption pulses to minimize fragmentation of C_{60} , in contrast to MW peak powers for traditional ns pulsed lasers; 4) efficient collisional cooling by He; and 5) controllable, transient (~ 30 ms response time) C_{60} yield, enabling rapid subtraction of probe light intensity fluctuations from absorption signal.

* lee.richard.liu@gmail.com

† ye@jila.colorado.edu

approximately $5(1) \times 10^{10} \text{ cm}^{-3}$, based on the integrated intensity of the $8.4 \mu\text{m}$ band [13], rotational temperature of 100 K, and effective optical path length of $\sim 475 \text{ m}$.

Having characterized the yield of laser desorbed C_{60} , we now turn to C_{60} rotational and Doppler thermometry. In particular, the 532 nm photons may deposit energy primarily into certain (e.g., electronic) degrees of freedom, initializing the C_{60} molecules in a highly non thermal state [14]. In contrast, an oven source produces molecules in which all internal degrees of freedom are approximately thermalized. Therefore, a significant concern was that laser desorbed C_{60} might not be efficiently cooled. On the other hand, since vibration-to-translation energy transfer is expected to be more favourable for smaller vibrational energy gaps, larger molecules might be expected to vibrationally quench easily due to collisions [15]. Furthermore, thermalization may occur rapidly in larger molecules even in the absence of collisions due to efficient intramolecular vibrational energy redistribution (IVR) [16–19]. Our measurements indicate that thermalization proceeds efficiently for laser desorbed C_{60} . A second key question was whether C_{60} could be efficiently quenched by collisions with He instead of Ar. Previous work with a 900 K oven source of C_{60} found that Ar gave the largest cold C_{60} peak absorbance [8] and that He has the smallest rotational quenching cross section amongst all noble gases [9]. Furthermore, He is $10\times$ more thermally conductive than Ar, exacerbating the heat transfer from the 1 kW oven to the nearby cryogenic buffer gas cell. Nevertheless, He is highly desirable as a buffer gas due to its significant vapor pressure at 4 K, making it compatible with a helium cryostat. He buffer gas cooling is also expected to mitigate possible cluster formation at lower temperatures [20]. Therefore, it was crucial to prove that He buffer gas efficiently collisionally quenches laser desorbed C_{60} as well.

The liquid nitrogen cold finger and buffer gas cell temperatures were directly measured with Cernox thin film resistance cryogenic temperature sensors and silicon diodes to be 82 K. Residual heat loads, such as radiative and conductive coupling to the room temperature dewar walls, dominate the total heat load and prevent the temperature from reaching 77 K, even with the desorption laser inactive. The static pressure in the cell was measured directly with a capacitance manometer. Absorption spectra were measured for six J -values scattered across the thermally populated states $R(J = 66, 96, 126, 156, 186, 206)$ at various buffer gas pressures (330 – 410 mTorr), which we controlled by varying the buffer gas flow rate (80 – 130 sccm).

The rotational temperature was obtained from the integrated absorbance at each of the six measured $R(J)$ lines. Assuming negligible population in the vibrationally excited states, the integrated absorbances $I(J)$ are dominated by the rotational populations in the vibrational ground state. Hence, $I(J) = CS_J g_J e^{-E_J/kT_{rot}}$, where C is proportional to the total C_{60} population, S_J is the intrinsic line strength factor [21], g_J is the angu-

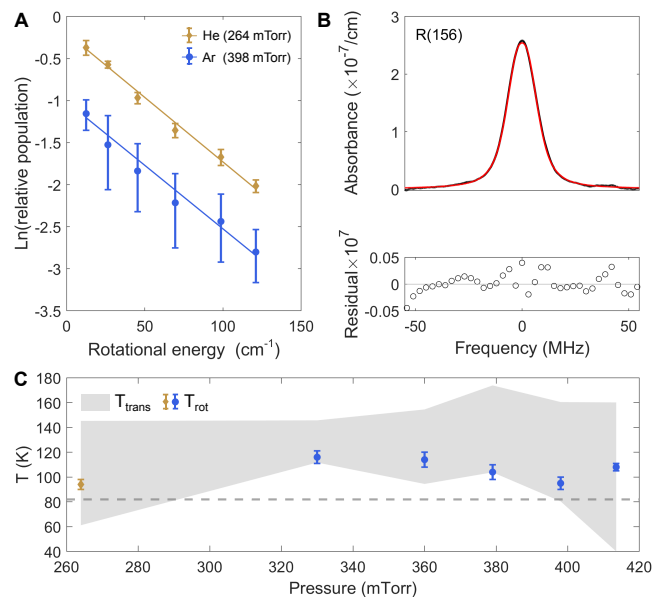


FIG. 3. Pressure-dependent Doppler and rotational thermometry of laser desorbed C_{60} in He and Ar buffer gas. A) Exemplary rotational temperature fits for C_{60} in Ar and He buffer gas. Note that He buffer gas cooling yields higher and more uniform molecular signal (as evident from the smaller error bars in the integrated absorption). B) Exemplary fit of $R(J = 156)$ absorption to rate equation, with residuals plotted below. C) Rotational and translational temperatures from Boltzmann analysis and rate equation fitting respectively, for a range of buffer gas pressures. The rotational temperatures lie within the error bounds of the fitted translational temperature. In addition, the coldest rotational temperatures approach 82 K, the temperature of the liquid nitrogen cold finger (horizontal dashed line). Note that He buffer gas cooling achieves the lowest rotational temperature, even at much lower pressure.

lar momentum degeneracy factor including lab-frame and molecular frame degeneracies for a spherical top and nuclear spin statistics weight [12], $E_J = BJ(J + 1)$ is the rotational energy in the vibrational ground state, k is the Boltzmann constant, and T_{rot} is the rotational temperature. Rearranging this equation gives $\text{Ln}(I(J)/(S_J g_J)) = \text{Ln}(C) - E_J/(kT_{rot})$. In this way T_{rot} can be extracted from the slope of a best-fit line to the logarithm of $I(J)/(S_J g_J)$, the relative populations per J multiplet component (Fig. 3A). For Ar buffer gas, we find that T_{rot} decreases with increasing pressure up until 400 mTorr, after which it rises again (Fig. 3C). The initial decrease in T_{rot} is expected: as pressure increases, the number of collisions experienced by C_{60} increases, thereby lowering the measured T_{rot} .

The rise in T_{rot} above 400 mTorr is also well understood. The total number of collisions a C_{60} molecule experiences before reaching the $8.4 \mu\text{m}$ beam is proportional to the product of buffer gas pressure and the time of flight from the target. Separately, we observed a decrease in the time of flight with increasing buffer gas flow,

suggesting that buffer gas “carries” desorbed C_{60} to the cavity axis at a speed that depends on the flow rate. Indeed, the time of flight ranges from a few to 10’s of milliseconds depending on the flow rate, which is intermediate between ballistic and diffusive transport. Therefore, while higher buffer gas flow increases pressure, it also decreases the C_{60} time of flight. Pressure in the cell begins to saturate at higher flow rates, possibly due to hydrodynamic effects [11, 22]. At sufficiently high flow rates therefore, the reduction in collision events due to time of flight overcomes the increase in collision rate due to pressure, and the total collision number drops with increasing flow rate. This is responsible for the measured increase in T_{rot} above 400 mTorr.

Since a considerable amount of averaging was needed to obtain sufficiently high signal to noise ratio for accurate line shape fitting, we obtained the translational temperature T_{trans} by globally fitting spectra measured for three selected J values ($J = 96, 156, 186$) to line shapes predicted by a semi-classical steady-state rate equation model discussed in Ref [9]. In particular, the model accounts for optical saturation of two counter propagating laser beams and J -dependent rotational quenching, which were crucial to obtain convergence of T_{trans} beyond simply fitting each line shape to an independent Voigt profile. We fix C_{60} -Ar collision cross section values from Ref [9] and allow the buffer gas temperature T_{BG} and T_{trans} to float, while constraining them to be equal ($T_{BG}=T_{trans}$) and independent of J . Here, T_{BG} affects the diffusion rate of C_{60} and the collision frequency. At our buffer gas pressures, we expect translational thermalization of C_{60} to occur in less than a hundred collisions [23], or a few microseconds, much shorter than the 10 ms timescale it takes for laser desorbed C_{60} to reach the interaction region. For each pressure value, T_{rot} was fixed by the independent rotational temperature fit described earlier. An exemplary fit for $R(J = 156)$ is shown in Fig. 3B.

For Ar buffer gas, we find that T_{trans} falls in the range 130 ± 30 K, with flat dependence on buffer gas pressure. The error bars reflect the fact that line shape fitting is generally insensitive to translational temperature, since inhomogeneous linewidth scales approximately as $\sqrt{T_{trans}}$. The translational and rotational temperatures agree within error bars and approach that of the liquid nitrogen cold finger, suggesting that rotational and translational degrees of freedom are nearly thermalized with each other and the buffer gas. We repeated the thermometry with He at a pressure of 265 mTorr and find that the fitted translational $T_{trans} = 103(42)$ K and rotational temperatures $T_{rot} = 94(4)$ K rival the lowest temperatures achieved with Ar, in spite of the much lower He pressure used (Fig. 3C). He buffer gas cooling also yielded a signal of cold C_{60} comparable to the highest C_{60} signal achieved with Ar cooling, as well as fractionally more stable C_{60} yield, indicated by the smaller error bars in (Fig. 3A). We attribute this stability to the suppression of C_{60} -buffer gas cluster formation. This hypothesis is

supported by the shallow interaction potential and lower near-dissociation threshold density of states of the C_{60} -He complex compared to C_{60} -Ar [20]. The large signal achieved with He buffer gas cooling also indicates that He collisions efficiently quench C_{60} vibrations, since transitions from excited vibrational states (vibrational “hot bands”) are expected to be red-shifted from transitions from the ground vibrational state (fundamental band) by $\sim 60 \text{ cm}^{-1}$ [24], and will not contribute to the resolved R branch features. With a greatly reduced heat load, He buffer gas cooling is fully compatible and in fact preferable for laser desorbed C_{60} .

As mentioned earlier, the apparently efficient thermalization of laser desorbed C_{60} should not come as a surprise. Intramolecular redistribution, particularly in a molecule as large as C_{60} , might redistribute the internal energy rapidly amongst internal degrees of freedom, even without buffer gas cooling. Indeed, thermal C_{60} sublimated from a 900 K oven source possesses 7.4 eV of vibrational energy, corresponding to the energy of three desorption photons at 532 nm. Smaller molecules, on the other hand, are expected to exhibit quenching bottlenecks due to large energy gaps and sparse spectrum of internal states [25, 26]. Our results are promising for laser desorption and subsequent collisional thermalization of other large molecules [6].

Having demonstrated efficient He buffer gas cooling of laser desorbed C_{60} , as well as the stable shot-to-shot C_{60} yield, we now turn to observing the extremely weak molecular absorption in the hitherto unseen $R(J = 0-29)$ spectral region. For $^{12}C_{60}$, since each carbon atom is a spinless, indistinguishable boson, the only allowed rotational states in the vibrational and electronic ground state are those which correlate to the totally symmetric irreducible representation in the icosahedral group. These correspond to $J = 0, 6, 10, 12, \dots$, with the remaining $R(J)$ transitions absent [12]. The striking icosahedral nuclear spin weights arise from the two-, three-, and five-fold discrete rotational symmetry axes of $^{12}C_{60}$, and are borne out in our observed spectra (Fig. 4). However, we also observe perturbations to the transition intensities and frequencies, perhaps due to high- J features from the Q branch, some accidentally degenerate vibrational combination state, or contamination from C_{60} isotopologues. The observation of these subtle perturbations is facilitated by the He buffer gas cooling, which provides stable shot-to-shot C_{60} yield and enables averaging of extremely weak molecular absorption signals.

In conclusion, we have demonstrated efficient cooling of laser desorbed C_{60} to below 100 K, which is sufficiently cold to observe the hitherto unseen $R(J = 0-29)$ transitions. This spectral region could be used for new tests of bosonic indistinguishability involving highly symmetric molecules [27–30]. In addition, the three orders of magnitude reduction in heat load of the laser desorption source compared to the oven source opens the door for cooling using a closed cycle He cryostat, which has much less cooling power than evaporating

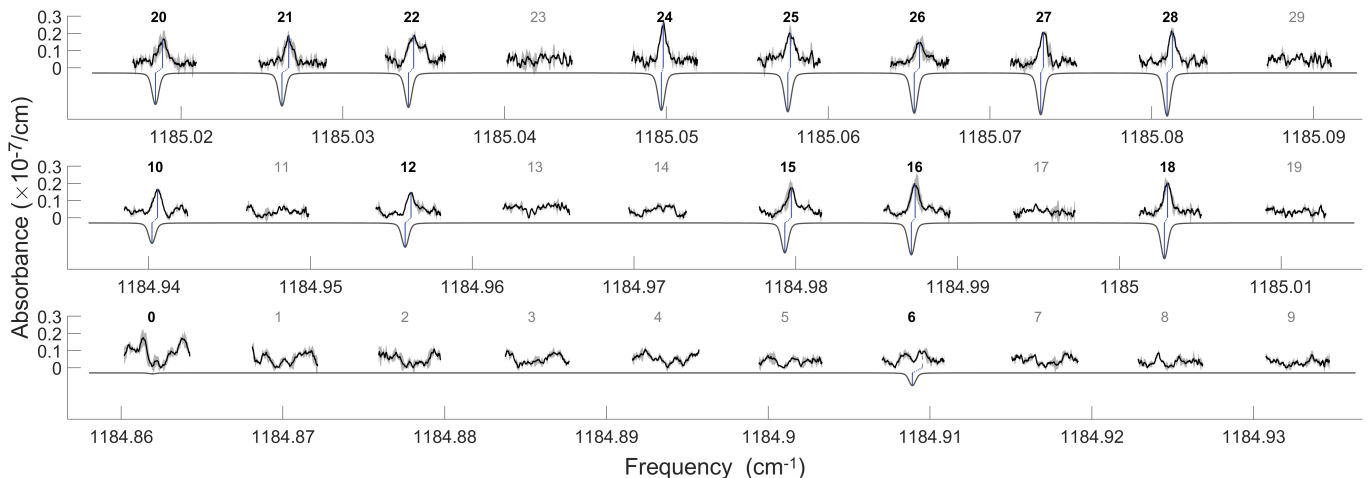


FIG. 4. **Complete $R(J = 0 - 29)$ absorption spectrum in the $8.4 \mu\text{m}$ rovibrational band of cold C_{60} .** Experimental data (black) is the average of 200-400 raw spectra, with the light gray error bands representing the point-wise standard deviation. Simulated spectrum (gray, inverted) derived from spectroscopic constants determined in Ref [8], assuming a rotational temperature of 100 K and including nuclear spin weights. Notably, the complete absence of many $R(J)$ transitions, as predicted by bosonic exchange statistics and the molecule’s icosahedral symmetry, is clearly visible. There is an increasing $\sim 5 - 15$ MHz blue-shift of experimental line centers (gray vertical lines) from the simulated spectrum as J decreases from $29 - 0$, continuing the trend seen in Ref [8]. Note, we tentatively assign $R(J = 6)$ to the higher frequency peak in the doublets (marked with a dash vertical line). Additional features at $J = 6$ and 22 and at very low J are deemed to be real.

liquid nitrogen. At the 4 K temperature achievable by a He cryostat, C_{60} population in the first 30 rotational levels in the electronic-vibrational ground state increases by two orders of magnitude, opening the door to understanding the origin of spectral perturbations, as well as providing a tantalizing route toward quantum state preparation of gas phase C_{60} at high density. We note that large molecules such as C_{60} are not amenable to the traditional approach of laser cooling due to their large mass (requiring correspondingly many more photon scattering events) and density of vibrational states (increasing the number of lasers required to “repump” vibrational populations), although a scheme involving chemical functionalization of a fullerene has been theoretically proposed [31]. Thus, laser desorption of C_{60} opens up a new class of molecules to quantum science.

We thank Adam Ellzey for technical assistance; the COSINC Fabrication facility at CU Boulder, particularly Dylan Bartusiak; and Jutta Toscano for the inspiration to pursue laser desorption of C_{60} . We thank Jacob Higgins and Baruch Margulis for providing useful comments on the manuscript. Funding support for this work is provided by AFOSR (FA9550-19-1-0148); NSF QLCI (QLCI OMA-2016244); NSF (Phys-1734006) and NIST. Support is also acknowledged from the U.S. Department of Energy, Office of Science, National Quantum Information Science Research Centers, Quantum Systems Accelerator. D.R. acknowledges support from the Israeli CHE Quantum Science fellowship, and is an awardee of the Weizmann Institute National Postdoctoral Award Program for Advancing Women in Science. Y.-C.C. and D.J.N. acknowledge support from the DOE (DE-FG02-09ER16021) and NSF (CHE 2053117).

-
- [1] L. R. Liu, D. Rosenberg, P. B. Changala, P. J. Crowley, D. J. Nesbitt, N. Y. Yao, T. V. Tscherbul, and J. Ye, *Science* **381**, 778 (2023).
 - [2] F. Schulz, M. Ijäs, R. Drost, S. K. Hämäläinen, A. Harju, A. P. Seitsonen, and P. Liljeroth, *Nature Physics* **11**, 229 (2015).
 - [3] R. Sawant, J. A. Blackmore, P. D. Gregory, J. Mur-Petit, D. Jaksch, J. Aldegunde, J. M. Hutson, M. R. Tarbutt, and S. L. Cornish, *New Journal of Physics* **22** (2020).
 - [4] M. Zeppenfeld, “A robust framework for quantum computation using quasi-hidden molecular degrees of freedom,” (2023), arXiv:2311.14133 [physics.atom-ph].
 - [5] V. V. Albert, E. Kubischta, M. Lemesko, and L. R. Liu, “Topology and entanglement of molecular phase space,” (2024), arXiv:2403.04572 [quant-ph].
 - [6] B. Spaun, P. B. Changala, D. Patterson, B. J. Bjork, O. H. Heckl, J. M. Doyle, and J. Ye, *Nature* **533**, 517 (2016).
 - [7] P. B. Changala, B. Spaun, D. Patterson, J. M. Doyle, and J. Ye, *Applied Physics B: Lasers and Optics* **122**, 1 (2016).
 - [8] P. Bryan Changala, M. L. Weichman, K. F. Lee, M. E. Fermann, and J. Ye, *Science* **363**, 49 (2019).
 - [9] L. R. Liu, P. B. Changala, M. L. Weichman, Q. Liang,

- J. Toscano, J. Kłos, S. Kotochigova, D. J. Nesbitt, and J. Ye, *PRX Quantum* **3**, 030332 (2022).
- [10] J. Weinstein, R. DeCarvalho, T. Guillet, B. Friedrich, and J. M. Doyle, *Nature* **255**, 242 (1998).
- [11] D. Patterson and J. M. Doyle, *The Journal of Chemical Physics* **126**, 154307 (2007).
- [12] P. R. Bunker and P. Jensen, *Molecular Physics* **97**, 255 (1999).
- [13] S. Iglesias-Groth, F. Cataldo, and A. Manchado, *Monthly Notices of the Royal Astronomical Society* **413**, 213 (2011).
- [14] D. Burgess, R. R. Cavanagh, and D. S. King, *The Journal of Chemical Physics* **88**, 6556 (1988).
- [15] H. Du, D. J. Krajnovich, and C. S. Parmenter, *Journal of Physical Chemistry* **95**, 2104 (1991).
- [16] C. S. Parmenter, *Journal of Physical Chemistry* **86**, 1735 (1982).
- [17] R. E. Smalley, *Journal of Physical Chemistry* **86**, 3504 (1982).
- [18] R. E. Smalley, *Annual Review of Physical Chemistry* **34**, 129 (1983).
- [19] D. J. Nesbitt and R. W. Field, *Journal of Physical Chemistry* **100**, 12735 (1996).
- [20] J. Kłos, E. Tiesinga, and S. Kotochigova, *Scientific Reports* **14** (2024).
- [21] G. Herzberg, *Molecular Spectra and Molecular Structure II Infrared and Raman of Polyatomic Molecules* (D. Van Nostrand company, inc., 1945).
- [22] J. F. Barry, E. S. Shuman, and D. Demille, *Physical Chemistry Chemical Physics* **13**, 18936 (2011).
- [23] B. Friedrich, *COLD MOLECULES: Theory, Experiment, Applications* (CRC Press Taylor and Francis Group, 2009).
- [24] H. Wang and M. S. Daw, *Computational Materials Science* **146**, 70 (2018).
- [25] A. Sinha, M. C. Hsiao, and F. F. Crim, *Journal of Chemical Physics* **92**, 6333 (1990).
- [26] A. Sinha, J. D. Thoemke, and F. F. Crim, *Journal of Chemical Physics* **96**, 372 (1992).
- [27] M. D. Angelis, G. Gagliardi, L. Gianfrani, and G. M. Tino, *Physical Review Letters* **76**, 2840 (1996).
- [28] G. Modugno, M. Inguscio, and G. M. Tino, *Physical Review Letters* **81**, 4790 (1998).
- [29] D. Mazzotti, P. Cancio, G. Giusfredi, M. Inguscio, and P. D. Natale, *Physical Review Letters* **86**, 1919 (2001).
- [30] P. C. Pastor, I. Galli, G. Giusfredi, D. Mazzotti, and P. D. Natale, *Physical Review A* **92**, 063820 (2015).
- [31] J. Kłos and S. Kotochigova, *Physical Review Research* **2**, 1 (2020).